RSC Advances




ROYAL SOCIETY OF CHEMISTRY

www.rsc.org/advances

Journal Name

RSCPublishing

ARTICLE

# Rigid triarylamine donor-π-acceptor porphyrin dyes and their application in dye-sensitized solar cells.

Cite this: DOI: 10.1039/x0xx00000x

Received 00th January 2012,
Accepted 00th January 2012

DOI: 10.1039/x0xx00000x

www.rsc.org/

Yongzhu Zhou[abc], Nicholas A. Lee[c], Ken T. Ngo[c], Xiao Peng[ab], Yaqing Feng[ab]*, Jonathan Rochford[c]*

Three donor-π-acceptor porphyrin dyes bearing a variety of rigid triarylamine donor groups were synthesized for application as photosensitizers in $TiO_2$ based dye-sensitized solar cells (DSSCs). Compared with the "naked" porphyrin **ZnP**, i.e. having no triarylamine moiety, broadened and red-shifted spectral features were exhibited by the triaylamine porphyrin sensitizers **ISB-ZnP**, **CZ-ZnP**, and **IDB-ZnP** where ISB = 5-phenyliminostilbene, CZ = 5-phenylcarbazole, and IDB = 5-phenyliminodibenzyl. Percentage power conversion efficiencies (η) and incident photon-to-current conversion efficiencies (%IPCE) in DSSC devices show the trend **ISB-ZnP** < **ZnP** < **CZ-ZnP** < **IDB-ZnP**. Inferior performance of the **ISB-ZnP** dye is attributed to its weaker adsorption to the $TiO_2$ film, which is roughly half that of **ZnP**. In contrast, introduction of the CZ and IDB electron donors is demonstrated to promote a better performance than the "naked" **ZnP** porphyrin. The best performance was observed for the **IDB-ZnP** device reaching a power conversion efficiency of η = 3.62 % under AM 1.5 irradiation conditions with a corresponding %IPCE maximizing at 48% for both Soret band (450 nm) and Q band (570 nm) photoexcitation.

## Introduction

Due to the low cost and high power conversion efficiencies, dye-sensitized solar cells (DSSCs) have attracted significant attention as alternatives to conventional photovoltaic devices based on silicon.[1, 2] In the early years of DSSC development research was focused mainly on the development of metal complexes as sensitizers inspired by the N3 and N719 dyes.[3-5] While ruthenium based sensitizers have offered great redox stability in DSSC devices, there has always been environmental concerns with respect to their large scale application.[6] For this reason organic photosensitizers, inspired by the porphyrin, chlorin and bacteriochlorin pigments found in the light harvesting antenna of photosystem II, have earned much interest.[7-12] Organic photosensitizers have a greater capacity for light absorption than the metal-to-ligand charge-transfer (MLCT) based visible absorption of ruthenium based photosensitizers and in recent years, due to enhanced steric and electronic molecular engineering, have competed successfully with the most efficient metal based DSSC devices.[13] A wide variety of organic dyes such as porphyrins, [14-18] coumarins,[19-21] perylene,[22, 23] phthalocyanines,[24] triarylamines,[25, 26] and carbazoles[26, 27] have been developed as successful alternatives to ruthenium(II) based sensitizers for use in DSSCs, however, the porphyrin chromophore remains the most widely studied system due to the combination of its highly evolved synthetic access and favorable optical, photophysical, electrochemical properties.[28, 29] Not only does the porphyrin chromophore exhibit multiple strong absorption bands in the visible region, but its redox and photophysical properties can be finely tuned by functionalization at either of its four *meso* or eighth *beta* positions.[30-32] The most celebrated application of porphyrins in a DSSC to date is the work of Yella et al. where the ethynyl conjugated triphenylamine porphyrin YD-o-C8 donor-π-acceptor system has achieved an overall power conversion efficiency of η = 12.3% in full sunlight.[13, 18] In this particular case the strong tendency of the planar porphyrin macrocylce to π-aggregate at the $TiO_2$ surface was resolved by introducing bulky alkyl substituents to provide considerable steric hindrance while also maximizing photocurrent generation by preventing charge recombination from the reduced $TiO_2$ conduction band and the oxidized $[Co(bpy)_3]^{3+}$ mediator.[33] Similarly, Aljarilla,[34] Fan,[35] and Zegkinoglou[36] have synthesized porphyrin dyes bearing the carbazole moiety as a redox active substituent in a donor-π-acceptor structure. Wang has recently introduced the triarylamines IDB (5-phenyl-iminodibenzyl) and ISB (5-phenyl-iminostilbene) as semi-rigid electron donating groups in conjugation with the simple thienyl cyanoacrylic acid acceptor.[37] A respectable power conversion efficiency of η = 5.83% was observed for the ISB donor leading

to the conclusion that the semi-rigid donor structure contributes to a greater charge injection efficiency and an overall improvement in DSSC performance. In the current study we wanted to test the hypothesis that expansion of the covalent aryl bridging linkage of the carbazole donor would lead to an overall improvement in DSSC performance utilizing a donor-π-acceptor porphyrin design. Three new porphyrin dyes are here presented with the rigid triarylamine electron donors CZ (5-phenyl-carbazole), ISB and IDB introduced at the *meso* position of porphrin ring (Figure 1). The "naked" photosensitizer zinc(II)-15-(4-carboxyphenyl)-10,20-diphenylporphyrin (**ZnP**) lacking a *meso*-functionalized triarylamine electron donor was studied as a reference system. Structural, electronic, photophysical and computational properties of these systems were investigated by $^1$H-NMR and mass spectroscopies, UV-Vis electronic absorption and fluorescence emission spectroscopies, time-dependent density functional theory (TDDFT), cyclic voltammetry, photocurrent-voltage and electrochemical impedance measurements.

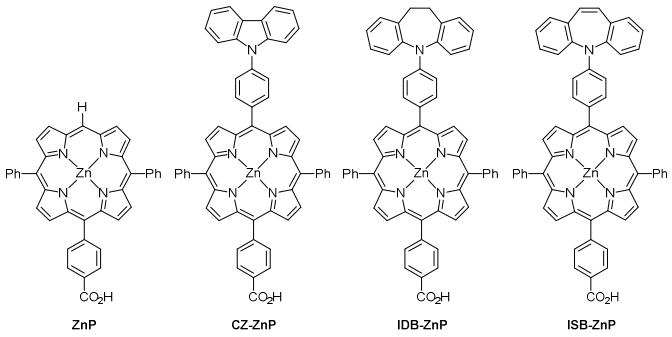


Figure 1. Molecular structures of the **ZnP**, **CZ-ZnP**, **IDB-ZnP** and **ISB-ZnP** dyes.

## Results and discussion

### Synthesis

Three rigid triarylamine porphyrin dyes were synthesized to afford the target photosensitizers **CZ-ZnP**, **IDB-ZnP** and **ISB-ZnP** alongside the reference dye **ZnP** (Scheme 1). The porphyrin precursors dipyrromethane, 5-phenyldipyrromethane and 5-(4-methoxycarbonylphenyl) dipyrromethane were synthesized according to the literature.[38] The rigid triarylamine aldehydes **1**, **2** and **3** were synthesized by a Buchwald-Hartwig type C-N coupling reaction between *p*-iodobenzaldehyde and the appropriate diarylamine in 52%, 62% and 67% yield, respectively, with a $Pd(OAc)_2$/DPEPhos catalyst in THF. This latter method proved more efficient than the previously reported Vilsmeier-Haack strategy.[37] The *meso*-substituted porphyrin intermediates **4**, **5** and **6** were subsequently prepared by a standard MacDonald type 2+2 condensation reaction. Although the yields of **4**, **5** and **6** were low due to scrambling reactions, sufficient quantities of sensitizer were isolated to proceed with the subsequent zinc(II) insertion and ester hydrolysis steps. The **ZnP** reference dye was synthesized in a similar manner.

### UV-Vis electronic absorption and fluorescence emission spectroscopy.

UV-Vis electronic absorption spectra of the porphyrin dyes recorded in dichloromethane are presented in figure 2a. All of

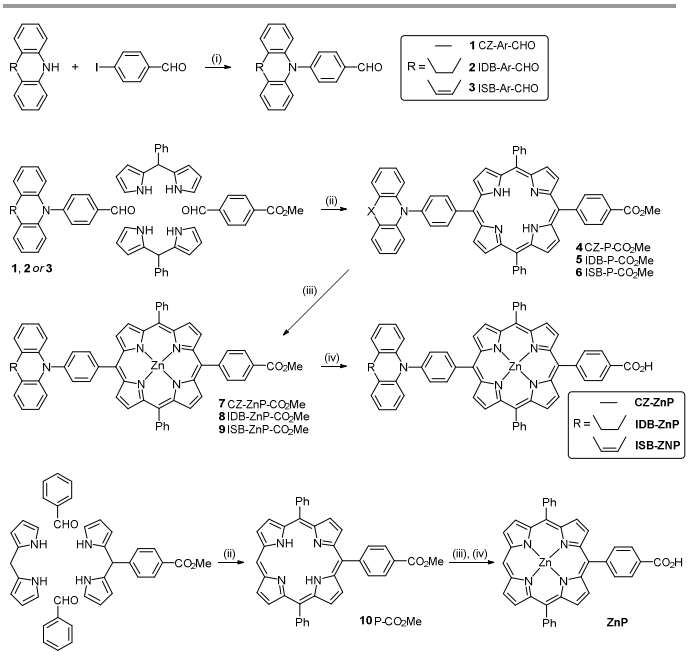


Scheme 1. The synthetic routes for **CZ-ZnP**, **IDB-ZnP**, **ISB-ZnP** and **ZnP**. Reaction conditions: (i) $Pd(OAc)_2$, $Cs_2CO_3$, 18-crown-6, DPEPhos, THF (ii) (a) TFA, $CH_2Cl_2$ (b) DDQ, $NEt_3$ (iii) $Zn(OAc)_2{\cdot}2H_2O$, $CHCl_3$, $CH_3OH$ (iv) (a) aq. KOH/THF/$C_2H_5OH$, (b) aq. HCl.

the dyes exhibit typical features of a porphyrin chromophore with a strongly absorbing Soret band ($S_0 \rightarrow S_2$) band in the 410 - 430 nm spectral region with associated molar extinction coefficients in the range of 2.34 x $10^5$ – 5.16 x $10^5$ $M^{-1}$ $cm^{-1}$. The less intense Q(0,1) and Q(0,0) bands (vibronic bands within the $S_0 \rightarrow S_1$ electronic transition) are observed in the spectral range 530 - 570 nm with molar extinction coefficients varying from 0.40 x $10^4$ - 7.68 x $10^4$ $M^{-1}$ $cm^{-1}$ (Table 1). As anticipated, due to introduction of the electron rich triarylamine substitutents, noticeable red-shifts of the Soret (7 – 10 nm) and Q (6 – 51 nm) bands are observed in each of the **CZ-ZnP**, **IDB-ZnP** and **ISB-ZnP** porphyrins relative to **ZnP**. The red-shift of the Soret bands is slight most likely due to the orthogonal orientation between the *meso*-aryl and central porphine ring systems. The same Soret bands do show a significant decrease in their molar extinction coefficients however, relative to the 'naked' **ZnP** system, with a concomitant broadening of their full-width half-maxima (fwhm). This suggests significant vibronic coupling between the triarylamine donors and the porphyrin ring system and is also favorable for enhanced light harvesting over a wider spectral range than **ZnP** (*vide infra*).[39] Interestingly, **ISB-ZnP** shows the strongest decrease and broadening of its Soret band for the series (ε = 3.54 x $10^5$ $M^{-1}$ $cm^{-1}$; fwhm = 1,336 $cm^{-1}$) likely due to its extended π-conjugation across the back of the ISB donor. Figure 2b shows

the normalized absorption spectra of the porphyrin photosensitizers adsorbed on optically transparent 5 µm thick mesoporous $TiO_2$ films. The Soret and Q bands on $TiO_2$ films are comparable to their solution phase spectra in figure 1a with a slight broadening possibly due to monolayer aggregation at the $TiO_2$ interface.[40] Encouragingly, from a light harvesting perspective, relatively strong Q band absorption is observed for all dyes adsorbed on the mesoporous $TiO_2$ films.

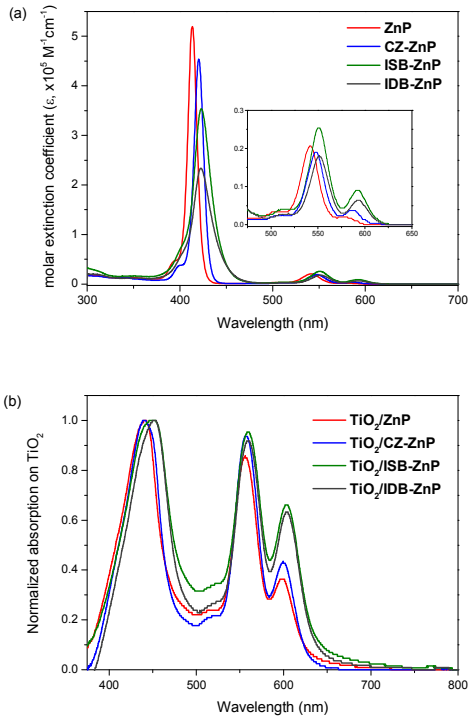


**Figure 2.** Absorption spectra of the porphyrin dyes recorded at 298 K in **(a)** dichloromethane and **(b)** adsorbed on optically transparent 5 µm thick $TiO_2$ films.

Fluorescence emission spectra were recorded in acetonitrile solvent to best reproduce the solvation conditions in a DSSC device. Typical for a *meso*-tetraphenyl porphyrin system, two distinct fluorescence bands are observed which arise from the Q(0,0)* and Q(0,1)* vibrationally resolved transitions (Fig. 3). All triarylamine substituted porphyrins show a stronger Q(0,0)* band relative to the **ZnP** system resulting in a slight increase in their fluorescence quantum yields. This may be as a result of increased molecular rigidity relative to the "naked" **ZnP** system. The **ISB-ZnP** system displays the largest quantum yield of the series at $\Phi_{fl}$ = 0.0020 (Table 1). Such low fluorescence quantum

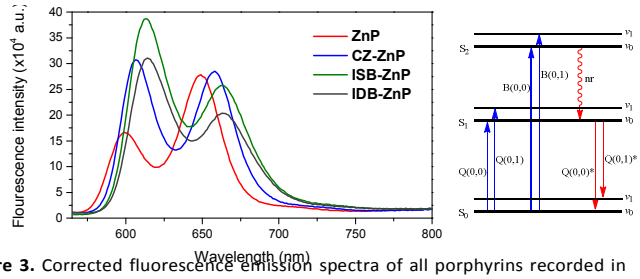


**Figure 3.** Corrected fluorescence emission spectra of all porphyrins recorded in argon degassed acetonitrile at 298 K. Peak areas are relative to the calculated quantum yields (re. Table 2). A schematic (right) is included to explain the origin of the higher energy Q(0,0)* and lower energy Q(0,1)* vibrationally resolved emission bands within the $S_1 \rightarrow S_0$ electronic transition. Q-band ($S_0 \rightarrow S_1$) and Soret (aka B) band ($S_0 \rightarrow S_2$) transitions are also included for reference.

yields are typical of the porphyrin macrocycle which has a strong tendency for non-radiative decay due to vibrational freedom of the macrocycle.

**Table 1.** UV-Vis electronic absorption and fluorescence emission data.

| Dyes | Absorption/nm (ε/x10$^5$ M$^{-1}$cm$^{-1}$)[a] | Emission/nm ($\Phi_{fl}$)[bc] |
|---|---|---|
| **ZnP** | 414 (5.16), 542 (0.22) | 600, 649 (0.0013) |
| **CZ-ZnP** | 420 (4.54), 548 (0.19), 586 (0.04) | 606, 658 (0.0016) |
| **IDB-ZnP** | 422 (2.34), 552 (0.19), 593 (0.77) | 613, 663 (0.0016) |
| **ISB-ZnP** | 423 (3.54), 551 (0.26), 592 (0.10) | 614, 664 (0.0020) |

[a]recorded in $CH_2Cl_2$ at room temperature. [b]recorded in acetonitrile under 1 atm $N_2$ at room temperature. [c]fluorescence data is corrected for excitation intensity ($\lambda_{exc}$ = 555 nm) and detector response.

## Computational analysis

To help guide interpretation of electrochemical data (*vide infra*), in correlation with the UV-Vis electronic absorption spectra, computational analysis was conducted on each of the porphyrin photosensitizers. Geometry optimization was first carried out by density functional theory (DFT) using the polarizable continuum model (PCM) with the dielectric constant of dichloromethane[41] where the rB3LYP hybrid exchange-correlation functional[42, 43] and 6-31g** basis set[44, 45] was used for all atoms. A vibrational frequency analysis coupled with the PCM model was carried out in order to confirm the minimum-energy geometry in solution. Electronic transitions contributions and oscillator strengths were subsequently determined by time-dependent density functional theory (TD-DFT).[46] Molecular orbital energies with frontier orbital images are presented in figure 4 with an exemplar TD-DFT predicted UV-Vis spectrum presented in figure 5 for the **IDB-ZnP** dye. A comprehensive summary of all TD-DFT data

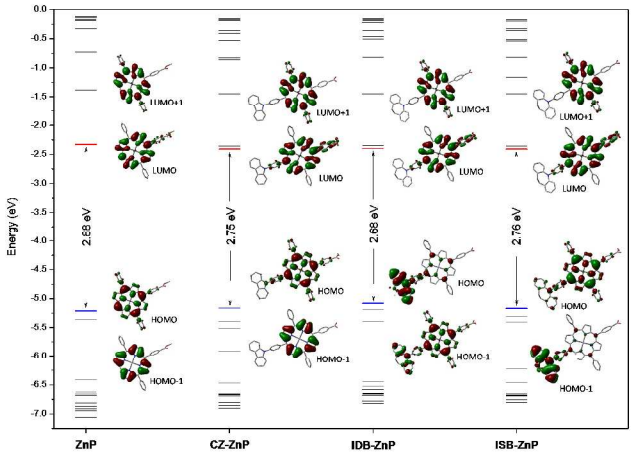


**Figure 4.** Molecular orbital energy level diagram for **ZnP** and the rigid triarylamine porphyrin dyes calculated using DFT (rB3LYP/6-31g**/dichloromethane PCM). HOMO and LUMO levels are highlighted in blue and red, respectively, with theoretical band gaps (eV) included for comparison. Electron occupancy is not displayed, and only select frontier orbital images are included for clarity.

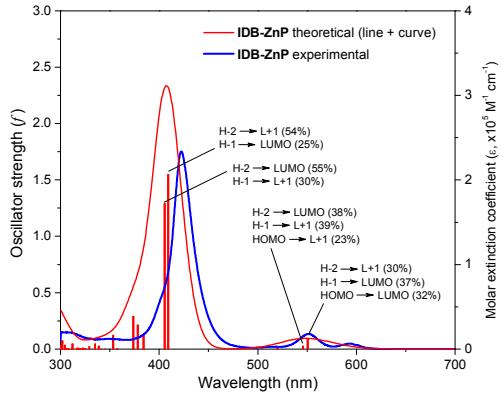


**Figure 5.** Overlay of theoretical (line & curve) and experimental spectra for the **IDB-ZnP** dye calculated/recorded in dichloromethane PCM/solvent, respectively. Electronic transitions and major contributions responsible for the Soret and Q band absorptions are also highlighted.

is provided in the supporting information for each dye. A closer look at the DFT optimized dye geometries is presented in figure 6. Interestingly, all triarylamine porphyrins show a slight ruffling of the porphyrin macrocycle relative to **ZnP** which likely contributes to the slight broadening and red-shift of their Soret bands.[47] Furthermore, comparison of the triarylamine donor optimized geometries in figure 6 illustrates the non-planarity of the rigid IDB and ISB aryl groups relative to CZ. This effect may inhibit π-delocalization onto the IDB ans ISB phenyl groups enhancing their electron donating capacity towards the porphyrin ring. This hypothesis is consistent with the trend in oxidation potentials observed experimentally via cyclic voltammetry studies below.

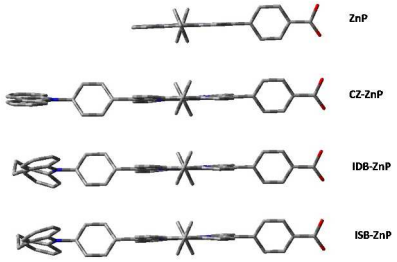


**Figure 6.** Side-on perspective view of DFT optimized geometries for **ZnP** and the rigid triphenylamine-porphyrin photosensitizers illustrating the non-planar geometry of both IDB and ISB triarylamine donors.

## Electrochemical properties

The electrochemical properties of all porpyrins were investigated by cyclic voltammetry (CV) to assess their potential for application in a $TiO_2$ based DSSC device. Critical for this application, the excited state oxidation potential of the photosensitizer must be more negative than the $TiO_2$ semiconductor conduction band ($E_{CB}$ = -0.50 V vs. NHE) for an exergonic charge-transfer photocurrent generation. Similarly, the excited state reduction potential of the photosensitizer must be more positive than the $2I^- \rightarrow I_2^{\bullet-}$ oxidation reaction within the DSSC $I_3^-/I^-$ redox mediator solution to facilitate dye regeneration.[48, 49] Unfortunately the $2I^- \rightarrow I_2^{\bullet-}$ oxidation reaction can only be estimated as < +0.93 V vs. NHE.[49, 50] In fact, the iodide oxidation potential is often misquoted as the triiodide reduction $E(I_3^- \rightarrow 3I^-)$ = +0.35 V which occurs at the Pt counter electrode and is responsible for the observed $V_{OC}$ based upon the relationship $V_{OC} = E(I_3^- \rightarrow 3I^-) - E_{Fermi}(TiO_2)$.[48, 49] Of course, reversible oxidation and reduction processes are also favoured to impart increase stability and high turnover number of the photosensitizer in a functional device. Cyclic voltammograms of all porphyrins recorded in *N*,*N*-dimethylformamide are presented in figure S21 and their data summarized in Table 2 in reference to the SCE electrode. All triarylamine porphyrins show a reversible first oxidation potential in contrast to the quasi-reversible nature of the **ZnP** first oxidation at +0.76 V. Oxidation of both **IDB-ZnP** and **ISB-ZnP** occurs at +0.74 V implying that they are slightly more electron rich than **CZ-ZnP** which displays its first oxidation potential at +0.82 V. A second quasi-reversible oxidation is observed for all triarylamine porphyrins in the range +0.94 to +1.02 V. All porphyrins in the series display three reductions, the first of which occurs in the narrow range of -1.41 V to -1.43 V implying that there is little change in energy of the porphyrin π* based LUMO energy level upon introduction of the various triarylamine electron donating groups. This is consistent with DFT calculations due to the limited π-conjugation across the orthogonal porphyrin and *meso*-aryl substituents.

**Table 2.** Electrochemical properties of the porphyrin dyes.[a]

| Dyes | $E_{ox}$ (V vs. SCE) | $E_{red}$ (V vs. SCE) | $E_{bg}$ (eV)[b] | $E_{0\text{-}0}$ (eV)[c] |
|---|---|---|---|---|
| **ZnP** | +1.15, +0.96, +0.76 | -1.43, -1.80, -1.97 | 2.19 | 2.11 |
| **CZ-ZnP** | +1.02, +0.82 | -1.41, -1.79, -1.95 | 2.22 | 2.08 |
| **IDB-ZnP** | +0.94, +0.74 | -1.43, -1.83, -1.96 | 2.17 | 2.06 |
| **ISB-ZnP** | +0.96, +0.74 | -1.42, -1.83, -1.96 | 2.17 | 2.06 |

[a]recorded in 0.1 M $Bu_4NPF_6$ *N,N*-dimethylformamide electrolyte.
[b]electrochemical band-gap ($E_{bg} = E_{ox} - E_{red}$) [c]optical $S_0(v_0)\rightarrow S_1(v_0)$ band-gap

The photosensitizer excited-state oxidation, $E(S^+/S^*)$, and reduction, $E(S^-/S^*)$, potentials can be estimated by consideration of the absorbed photon energy according to equations 1 and 2.

$$E(S^+/S^*) = E(S^+/S) - \Delta E_{0\text{-}0}(S/S^*) \quad \text{eqn. 1}$$

$$E(S^-/S^*) = E(S^-/S) + \Delta E_{0\text{-}0}(S/S^*) \quad \text{eqn. 2}$$

Here, 'S' symbolizes the ground state photosensitizer, '$S^+$' and '$S^-$' the oxidized and reduced forms of the photosensitizer, S* the singlet excited state of the photosensitizer, and $\Delta E_{0\text{-}0}$ the 0-0 energy of the $S_0\rightarrow S_1$ electronic transition. $\Delta E_{0\text{-}0}$ may be estimated by determining the point of intersection between the normalized Q(0,0) absorption and Q(0,0)* emission bands. Alternatively, the electrochemically determined HOMO-LUMO band-gap $E_{bg}$ may be used although this is often overestimated relative to optical band gap (Table 3). Energy level alignment of all porphyrins is summarized in figure 7. Here sufficient driving forces are observed for excited-state charge-transfer oxidation to the $TiO_2$ conduction band, $\Delta G = |E(S^+/S^*) - E_{CB}(TiO_2)|$, and the subsequent dye regeneration by the iodide redox mediator.[34]

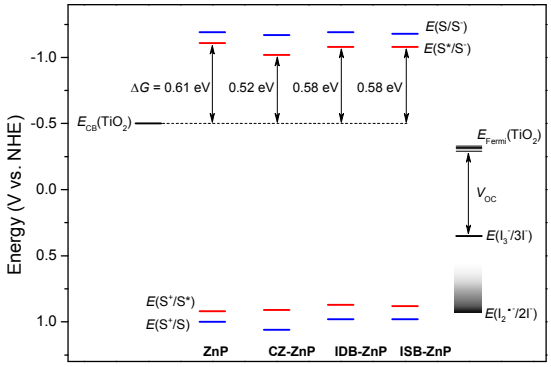


**Figure 7.** Energy level alignment of the porphyrin dyes relative to the $TiO_2$ conduction band ($E_{CB}$) and the iodide oxidation potential. Ground and excited state redox potentials are distinguished in blue and red, respectively. All potentials are referenced vs. NHE (SCE = +0.241 vs. NHE).

**Photovoltaic studies**

Dye-sensitized solar cells were fabricated according to standard methods using an FTO/$TiO_2$ sensitized photoanode, FTO/Pt cathode and a $I_3^-/I^-$ acetonitrile redox mediator electrolyte. Photocurrent density-voltage (*J-V*) curves are presented in figure 8. The surface coverage parameters of each dye (Γ, mol $cm^{-2}$) and detailed parameters of photovoltaic performance, i.e. short-circuit current density (*J*sc), open-circuit voltage (*V*oc), fill factor (*FF*), and power conversion efficiency (η), are summarized in table 3. The reference **ZnP** photosensitizer shows a power conversion efficiency of η = 3.01% while the **CZ-ZnP** and **IDB-ZnP** dyes show the best performance with η = 3.47% and 3.62%, respectively. This is primarily due to an increase in photocurrent with **CZ-ZnP** maximizing at $J_{SC}$ = 7.00 mA $cm^{-2}$. Although **IDB-ZnP** displays a slightly lower photocurrent ($J_{SC}$ = 6.93 mA $cm^{-2}$) its greater fill-factor (*FF* = 0.780) allows it to top the series of dyes studied. Interestingly, the **ISB-ZnP** photosensitizer displays a poorer performance than even the **ZnP** reference system with a power conversion efficiency of just 2.55 %. The lower $V_{OC}$ of **ISB-ZnP** of 640 mV is likely due to a lowering of the $TiO_2$ Fermi-level consistent with the poorer photocurrent observed ($J_{SC}$ = 5.92 mA $cm^{-2}$). To gain further insight into the photocurrent generation of each device their

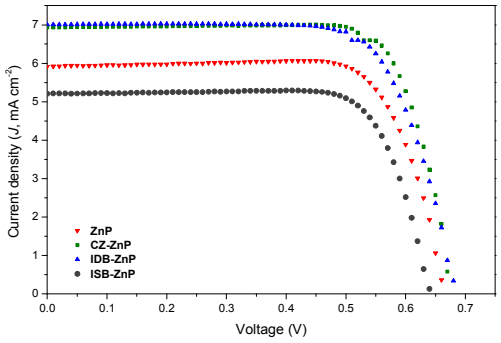


**Figure 8.** Photocurrent–voltage (*J-V*) plots of the porphyrin DSSC devices recorded under AM 1.5G simulated irradiation.

**Table 3**. Photovoltaic performance data of the four dyes in a DSSC device.

| Dyes | Γ ($10^{-8}$ mol $cm^{-2}$) | $V_{OC}$ (mV) | $J_{SC}$ (mA $cm^{-2}$) | *FF* | η (%) |
|---|---|---|---|---|---|
| **ZnP** | 6.7 | 660 | 5.92 | 0.770 | 3.01 |
| **CZ-ZnP** | 5.2 | 680 | 7.00 | 0.729 | 3.47 |
| **IDB-ZnP** | 5.7 | 670 | 6.93 | 0.780 | 3.62 |
| **ISB-ZnP** | 3.5 | 640 | 5.20 | 0.767 | 2.55 |

Light source: 100 mW $cm^{-2}$ AM 1.5G simulated solar light. Working area: 0.159 $cm^2$. Thickness: 15 mm. Dye bath: 0.3 mM EtOH solution. Electrolyte: 0.06 M LiI, 0.03 M $I_2$, 0.6 M 1,2-dimethyl-3-propylimidazolium iodide (DMPII), 0.5 M 4-tertbutylpyridine (TBP) in acetonitrile solution.

incident photon-to-current conversion efficiency (IPCE) spectra were measured (Figure 9). Consistent with the *J-V* plots, a lower photocurrent is observed across the entire visible spectrum for **ISB-ZnP** with a similar trend observed across the series, i.e. **ISB-ZnP** < **ZnP** < **CZ-ZnP** < **IDB-ZnP**. The improved light harvesting performance of **CZ-ZnP** and **IDB-ZnP** is consistent with their greater surface coverage relative to **ISB-ZnP**. In fact, both **CZ-ZnP** and **IDB-ZnP** display 48% IPCE maxima upon irradiation of both their Soret and Q-bands.

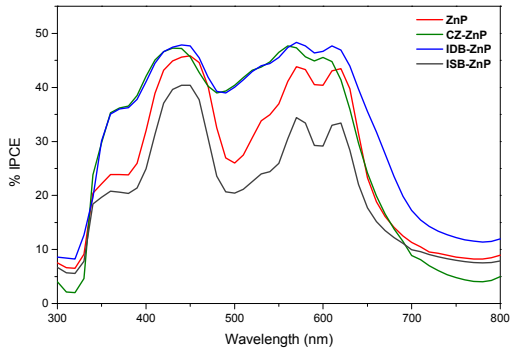


**Figure 9.** Percentage incident photon-to-current conversion efficiencies (%IPCE) recorded under monochromatic irradiation at 10 nm step intervals.

### Electrochemical impedance spectroscopy

To gain further insight into the influence of the rigid triarylamine substituents on DSSC photovoltaic performance electrochemical impedance spectroscopy was conducted to study interfacial charge-transfer resistance.[51] EIS analyses was performed in the dark at an applied bias of -0.6 V making the electronic and steric properties of each dye the only variable between each device. Nyquist plots are presented in figure 10. An electrochemical impedance Nyquist plot of a DSSC device typically contains three semicircles.[51-53] The high-frequency (leftmost) semicircle, associated with the Pt → $I_3^-$ interfacial charge-transfer processes, is usually of weak intensity (low resistance) and is here obscured by the larger mid-frequency semicircle. The latter is attributed to $TiO_2$ → $I_3^-$ interfacial charge recombination, here of prime importance. Finally, the low-frequency (right-most) semicircle, attributed to $I_3^-/I^-$ mass-transfer resistance, is also weak and is again mostly obscured by the intense mid-frequency signal.

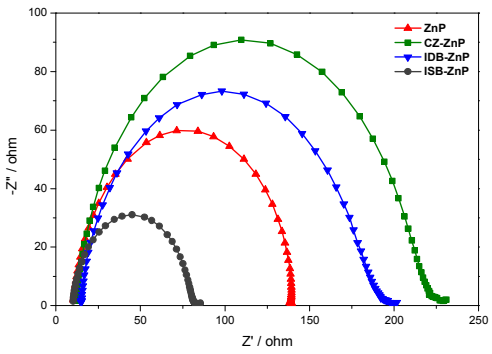


**Figure 10.** Electrochemical impedance Nyquist plots of porphyrin DSSC devices under a -0.6 V applied bias in dark conditions.

Dominance of the mid-frequency semicircle in the Nyquist plot confirms that $TiO_2$ → $I_3^-$ interfacial charge transfer is rate-determining and significantly influencing the overall device efficiency. Under the experimental conditions employed (-0.6 V bias in the dark), observation of a high resistance to $TiO_2$ → $I_3^-$ interfacial charge-recombination is favourable. This informs on the porosity of the $TiO_2$/porphyrin monolayer and its capacity for preventing performance deteriorating $TiO_2$ → $I_3^-$ charge-recombination. Consistent with having the lowest $V_{OC}$, power conversion efficiency and %IPCE of the series **ISB-ZnP** displays the least resistance to charge-recombination. Overall the Nyquist plots show that the $TiO_2$ → $I_3^-$ charge-recombination resistance increases in the order **ISB-ZnP** < **ZnP** < **IDB-ZnP** < **CZ-ZnP**. An identical trend is observed across the series for both $J_{SC}$ and $V_{OC}$ which suggests a similar trend in the $TiO_2$ Fermi level according to the relationship $E_F = V_{OC} - E(I_3^-/I^-)$. An increased $J_{SC}$ and $V_{OC}$ is anticipated for **CZ-ZnP** based upon its greater oxidation potential and hence greater driving force for dye regeneration via iodide oxidation. However, considering these electronic factors, a slightly higher power conversion efficiency is still observed for the **IDB-ZnP** photosensitizer consistent with its greater surface coverage and larger fill factor relative to **CZ-ZnP**. Therefore the trend in observed photovoltaic parameters and charge-recombination resistance for the triarylamine porphyrin sensitizers here studied goes beyond their electronic properties and can be attributed to a combination of dye surface coverage and possibly even triarylamine steric effects at the $TiO_2$-photosensitizer interface.

## Conclusions

In summary, three new porphyrin sensitizers containing the 5-phenyl-carbazole (CZ), 5-phenyl-iminodibenzyl (IDB) and 5-phenyl-iminostilbene (ISB) electron donors have been designed and synthesized for application in DSSCs. It was found that the **CZ-ZnP** and **IDB-ZnP** dyes exhibit an improved photovoltaic performance compared to the "naked" **ZnP** dye, which lacks a *meso*-substituted triarylamine electron donor. In contrast, the **ISB-ZnP** triarylamine photosensitizer displays a lower efficiency than **ZnP**. Using a combination of *J-V*, %IPCE and electrochemical impedance analysis the trend in DSSC device performance was found to correlate extremely well with the $J_{SC}$, $V_{OC}$ and $TiO_2$ → $I_3^-$ charge-recombination properties. As the electronic properties of each dye studied in solution were not deemed significantly different to cause such an effect, the differences observed in device performance are best attributed to surface coverage and steric factors which together control porosity and $I_3^-$ mass-transfer in the mesoporous $TiO_2$/porphyrin film. In conclusion, this study confirms the critical importance of both the electronic and structural characteristics of triarylamine electron donors when designing a DSSC photosensitizer and highlights the IDB triarylamine

donor as a promising alternative in the future design of original and versatile organic photosensitizers.

## Experimental section

### Materials and reagent

All reagents and solvents were obtained from commercial sources and used without further purification, unless otherwise noted. THF was dried prior to use by distillation over sodium using benzophenone as an indicator. $CH_2Cl_2$ was also freshly distilled prior to use. All chromatographic separations were carried out on silica gel (300-400 mesh or silica H) using $CH_2Cl_2$:petroleum ether solvent systems .

### Analytical measurements

$^1$H-NMR spectra were recorded in $CDCl_3$ or DMSO on Bruker AV400 spectrometer. The chemical shifts were reported in parts per million (δ) relative to the appropriate reference signal: residual chloroform ($\delta_H$ 7.26 ppm) or DMSO (the quintet centered at 2.50 ppm). High resolution MALDI-TOF mass spectra were recorded on a Bruker Autoflex TOF/TOF III instrument. UV-Vis electronic absorption spectra were recorded on a Shimadzu UV-1800 instrument. Although, acetonitrile is more suitable for mimicking DSSC conditions, molar extinction coefficients were determined in $CH_2Cl_2$ as complete dissolution of solids was not possible in acetonitrile. Emission spectra were recorded on a PTI Quantamaster 40 fluorimeter. Fluorescence quantum yields for all samples ($\Phi_{fl}$) were calculated by the optically dilute technique in argon degased acetonitrile solutions with ZnTPP used as a reference ($\Phi_{ref}$ = 0.033 in toluene) for all samples according to eqn. 3.

$$\Phi_{fl} = \left(\frac{A_s}{A_{ref}}\right)\left(\frac{I_s}{I_{ref}}\right)\left(\frac{\eta_{ref}}{\eta_s}\right)^2 \Phi_{ref} \quad \text{eqn. 3}$$

The subscript "s" refers to the sample and the subscript "ref" to the reference sample, A is the absorbance at the excitation wavelength, I is the integrated emission area, $\eta_s$ is the solvent refractive index of the unknown sample and $\eta_{ref}$ is the solvent refractive index of the reference sample. Excitation and emission slits were both set at 2 nm and an excitation wavelength of 555 nm was used for all samples. Cyclic voltammetry was conducted on a CH Instruments 620D potentiostat for all complexes. A standard three electrode cell was used with a supporting electrolyte of 0.1 M $Bu_4NPF_6$ in spectrophotometric grade *N,N*-dimethylformamide under an atmosphere of argon. The electrode assembly consisted of a glassy carbon disc working electrode (3-mm diameter), a Pt wire counter electrode and a non-aqueous reference electrode to minimize IR drop. The latter consisted of a Ag wire in the same 0.1 M $Bu_4NPF_6$ *N,N*-dimethylformamide electrolyte but separated by a porous vycor frit. The ferricenium/ferrocene redox couple was used as a pseudo reference and was added to each porphyrin electrolyte solution at the end of every experiment for in-situ calibration.

### Computational analysis

Geometry optimization was first carried out using density functional theory (DFT) with the rB3LYP hybrid exchange-correlation functional[42, 43] and 6-31g** basis set[44, 45] for all atoms as implemented in the Gaussian '09 program[54] using the polarizable continuum model (PCM) with the dielectric constant of dichloromethane.[41] A vibrational frequency analysis coupled with the PCM model was carried out in order to confirm the minimum-energy geometry in solution. Subsequent time-dependent density functional theory (TD-DFT) calculations were carried out on all compounds.[46] Finally, the percent contributions of atomic orbitals to molecular orbitals were calculated using the Gaussum software.[55]

### Absorption spectra on $TiO_2$ films

Absorption spectra of the sensitizers deposited on optically transparent $TiO_2$ films were measured with a Shimadzu UV-1800 spectrometer. The $TiO_2$ films with a typical thickness of 5 μm were dipped into 0.3 M ethanol solution of dyes for 15 min, then the sensitized films were rinsed with ethanol three times and air-dried before measurement of their absorption spectra.

### Measurement of surface coverage (Γ)

$TiO_2$ films with an area of 0.16 $cm^2$ and 16 mm thickness were dipped into 0.3 M ethanol dye solutions for 2 h and then thoroughly washed with ethanol to remove any excess physisorbed dye. The quantity of chemisorbed dye was estimated by desorption in 3 mL of 0.1 M EtONa solution. The absorption spectra of the EtONa solutions were then measured to obtain the surface coverage (Γ) via molar extinction coefficient data according to the standard method.[56]

### Fabrication of DSSCs and photovoltaic measurements

A $TiO_2$ sol-gel was prepared from P25 following a literature procedure.[57] The FTO/$TiO_2$ electrodes were prepared by screen printing on a pre-cleaned FTO glass. The film was then annealed to 325°C for 5 min, 375°C for 5 min, 450°C for 15 min, and 500°C for 15 min. Finally, the $TiO_2$ film was post-treated with an aqueous $TiCl_4$ solution (50 mM) at 70°C for 30 min, rinsed with ethanol, and annealed again at 500°C for 30 min. After the film was cooled to 100°C, the $TiO_2$ electrode was immersed into an ethanol solutions of the dye (0.3 mM) for 2 h. The sensitized electrode was rinsed thoroughly with ethanol and then air-dried. A sandwich cell consisting of the porphyrin sensitized $TiO_2$ working electrode and a Pt foil counter electrode was fabricated. The electrolyte (0.06 M LiI, 0.03 M $I_2$, 0.6 M 1,2-dimethyl-3-propylimidazolium iodide, and 0.5 M 4-tert-butylpyridine in acetonitrile) was injected between both working and counter electrodes. Upon fabrication the porphyrin based DSSCs were tested under simulated AM 1.5G irradiation (100 mW $cm^{-2}$) by photocurrent–voltage (*J-V*) analysis on a Keithley 2400 Source meter (solar AAA simulator, Oriel China, calibrated with a standard crystalline silicon solar). The percentage power conversion efficiency ($\eta$) was calculated according to equation 4:

$$\eta = \frac{P_{out}}{P_{in}} \times 100 = \frac{J_{SC}\, V_{OC}\, FF}{I_0} \times 100 \quad \text{eqn. 4}$$

where $J_{SC}$ is the short-circuit current density (mA $cm^{-2}$), $V_{OC}$ is the open-circuit voltage (V), *FF* is the fill-factor and $I_0$ the light flux (AM 1.5G). Photocurrent action experiments were performed on a commercial apparatus (Q Test Station 2000 IPCE Measurement System, CROWNTECH, USA) and incident photon-to-current conversion efficiencies were calculated according to equation 5:

$$\% \text{ IPCE} = 1240 \text{ x } \frac{I_{SC(\lambda)}}{I_{0(\lambda)}\,\lambda(nm)} \text{ x } 100 \qquad \text{eqn. 5}$$

where $I_{SC}(\lambda)$ is the monochromatic short circuit current, $I_0(\lambda)$ is the monochromatic light flux incident on the 0.16 $cm^2$ DSSC area and λ is the monochromatic excitation wavelength. Electrochemical impedance spectra of the DSSCs were recorded on a CH Instruments 760D potentionstat at a forward bias of -0.6 V under dark conditions at room temperature. The spectra were scanned in a frequency range of 0.1–$10^6$ Hz and an AC amplitude of 10 mV at room temperature.

**Synthesis of the photosensitizers**

**SYNTHESIS OF 1, 2 & 3**

The rigid triarylamine aldehydes **1**, **2** and **3** were prepared by coupling *p*-iodobenzaldehyde with the appropriate diarylamine which proved more efficient than the previously reported Vilsmeier-Haack preocedure.[37] Analytical data was identical to that reported in the literature and is summarize following the general procedure outlined for **1**. A solution of carbazole (334 mg, 2 mmol), 4-iodobenzaldehyde (557 mg, 2.4 mmol), palladium(II) acetate (22.4 mg, 0.1 mmol), DPEPhos (bis[(2-diphenylphosphino)phenyl] ether) (80.7 mg, 0.15 mmol), cesium carbonate (1.629 g, 2.5 mmol) and 18-crown-6 (26.4 mg, 0.1 mmol) in THF (50 mL) was refluxed for 5 h under argon atmosphere. The inorganic components were removed by filtration after cooling, the solvent was distilled under reduced pressure, then the crude product was purified by column chromatography to yield a white solid **1** (282 mg, 52%).$^1$H NMR (400 MHz, $CDCl_3$) δ: 10.12 (s, 1H, -CHO), 8.19 – 8.12 (m, 4H, Ar-H), 7.80 (d, *J* = 8.2 Hz, 2H, Ar-H), 7.51 (d, *J* = 8.2 Hz, 2H, Ar-H), 7.44 (t, *J* = 7.6 Hz, 2H, Ar-H), 7.34 (t, *J* = 7.4 Hz, 2H, Ar-H).

**2** a pale yellow solid (371 mg, 62%).$^1$H NMR (400 MHz, $CDCl_3$) δ 9.74 (s, 1H, -CHO), 7.62 (d, *J* = 8.8 Hz, 2H, Ar-H), 7.42 – 7.36 (m, 2H, Ar-H), 7.32 (s, 6H, Ar-H), 6.64 (d, *J* = 8.8 Hz, 2H, Ar-H), 3.01 (s, 4H, Ar-H).

**3** a light red solid (398 mg, 67%).$^1$H NMR (400 MHz,$CDCl_3$) δ: 9.70 (s, 1H, -CHO), 7.61 – 7.45 (m, 8H, Ar-H), 7.44 – 7.37 (m, 2H, Ar-H), 6.87 (s, 2H, Ar-H), 6.36 (d, *J* = 8.8 Hz, 2H, -CH=CH-).

**SYNTHESIS OF 4, 5 & 6**

The mixture of methyl-4-formylbenzoate (164 g, 1 mmol), **1** (271 mg, 1 mmol), and 5-phenyldipyrromethane (444 mg, 2 mmol) was condensed in dichloromethane (200 mL) with TFA (0.055 ml, 0.74 mmol) at room temperature for 4 h in the dark. DDQ (0.681 g, 3 mmol) was added, after which the mixture was stirred for 6 h at room temperature. TEA (3 ml) was added to quench the reaction. The reaction mixture was stirred for another 1 h at room temperature. The solvent was removed under reduced pressure. The residue was purified by silica gel column chromatography and recrystallization from $CH_2Cl_2$/n-Hexane gave **4** (34 mg, 4%).$^1$H NMR (400 MHz, $CDCl_3$) δ: 9.01 (d, *J* = 4.8 Hz, 2H, pyrr-H), 8.94 (d, *J* = 4.8 Hz, 2H, pyrr-H), 8.89 (d, *J* = 4.7 Hz, 2H, pyrr-H), 8.81 (d, *J* = 4.7 Hz, 2H, pyrr-H), 8.52 – 8.43 (m, 4H, Ar-H), 8.37 – 8.20 (m, 8H, Ar-H), 8.00 (d, *J* = 8.1 Hz, 2H, Ar-H), 7.88 – 7.78 (m, 8H, Ar-H), 7.59 (t, *J* = 7.6 Hz, 2H), 7.41 (t, *J* = 7.5 Hz, 2H, Ar-H), 4.12 (s, 2H, -COOMe), -2.73 (s, 2H, NH).MALDI-Tof: *m/z* calcd for $C_{58}H_{39}N_5O_2$, 837.31; found, 837.61[M]$^+$.

**5** (52 mg, 6%). $^1$H NMR (400 MHz, $CDCl_3$) δ 8.99 (t, *J* = 4.6 Hz, 2H, pyrr-H), 8.84 (d, *J* = 6.5 Hz, 4H, pyr-H), 8.76 (d, *J* = 4.8 Hz, 2H, pyrr-H), 8.44 (dd, *J* = 8.2, 3.1 Hz, 2H, Ar-H), 8.29 (dd, *J* = 8.5 Hz, 2 H, Ar-H), 8.26– 8.16 (m, 4H, Ar-H), 7.94 (dd, *J* = 8.6, 1.3 Hz, 2H), 7.82 – 7.68 (m, 8H, Ar-H), 7.39 (t, *J* = 7.6 Hz, 4H, Ar-H), 7.34 – 7.29 (m, 2H, Ar-H), 6.97 (d, *J* = 8.7 Hz, 2H), 4.11 (d, *J* = 3.9 Hz, 3H, -COOMe), 3.24 (s, 4H, -$CH_2CH_2$-), -2.75 (s, 2H, NH).MALDI-Tof: m/z calcd for$C_{60}H_{43}N_5O_2$, 865.34; found, 865.63[M]$^+$.

**6** (61 mg, 7%).$^1$H NMR (400 MHz, $CDCl_3$) δ 8.94 (d, 2H, pyrr-H), 8.85 – 8.78 (m, 4H, pyrr-H), 8.78 – 8.70 (m, 2H, pyrr-H), 8.43 (dd, *J* = 8.2, 2.2 Hz, 2H, Ar-H), 8.29 (d, *J* = 8.2 Hz, 2H, Ar-H), 8.20 (d, *J* = 6.3 Hz, 2H, Ar-H), 7.87 – 7.82 (m, 2H, Ar-H), 7.80– 7.71 (m, 8H, Ar-H), 7.65 – 7.55 (m, 4H, Ar-H), 7.48 – 7.48 (m, 2H, Ar-H), 7.05 (s, 2H, Ar-H), 6.68 (d, *J* = 8.7 Hz, 2H, -CH=CH-), 4.11 (d, *J* = 4.4 Hz, 3H, -COOMe), -2.78 (s, 2H, NH).MALDI-Tof: *m/z* calcd for $C_{60}H_{41}N_5O_2$, 863.32; found, 863.62[M]$^+$.

**SYNTHESIS OF 7, 8 & 9**

To a solution of porphyrin **4**, **5** or **6** (0.025 mmol) in $CHCl_3$ (20 ml) was added zinc(II) acetate dihydrate (22 mg, 0.10 mmol) in $CH_3OH$ (5 ml). The mixture was refluxed for 1 h. The solvent was removed under reduced pressure. The residue was purified by silica gel column chromatography and recrystallization from $CH_2Cl_2$/n-Hexane to give analytically pure product:
**7** (21 mg, 93%). $^1$H NMR (400 MHz, $CDCl_3$) δ: 9.12 (d, *J* = 4.7 Hz, 2H, pyrr-H), 9.05 (d, *J* = 4.7 Hz, 2H, pyrr-H), 9.00 (d, *J* = 4.7 Hz, 2H, pyrr-H), 8.91 (d, *J* = 4.7 Hz, 2H, pyrr-H), 8.45 (dd, *J* = 11.6, 8.2 Hz, 4H, Ar-H), 8.33 (d, *J* = 7.3 Hz, 2H, Ar-H), 8.30 – 8.23 (m, 6H, Ar-H), 7.99 (d, *J* = 8.2 Hz, 2H, Ar-H), 7.84 – 7.71 (m, 8H, Ar-H), 7.58 (t, *J* = 7.6 Hz, 2H, Ar-H), 7.40 (t, *J* = 7.4 Hz, 2H, Ar-H), 4.11 (s, 3H, -COOMe).MALDI-Tof: *m/z* calcd for $C_{58}H_{37}N_5O_2Zn$, 899.22; found, 899.14[M]$^+$.

**8** (21 mg, 92%) $^1$H NMR (400 MHz, $CDCl_3$) δ 9.12 – 9.07 (m, 2H, pyrr-H), 8.94 (m, 4H, pyrr-H), 8.86 (d, *J* = 4.6 Hz, 2H, pyrr-H), 8.41 (dd, *J* = 8.2, 3.0 Hz, 2H, Ar-H), 8.30 (dd, *J* = 8.2, 1.6 Hz, 2H, Ar-H), 8.25 – 8.18 (m, 4H, Ar-H), 7.93 (d, *J* = 7.7

Hz, 2H, Ar-H), 7.74 (m,8H, Ar-H), 7.38 (t, $J$ = 7.9 Hz, 4H, Ar-H), 7.31 (dd, $J$ = 11.1, 3.7 Hz, 2H, Ar-H), 6.96 (d, $J$ = 8.6 Hz, 2H, Ar-H), 4.09 (d, $J$ = 3.7 Hz, 3H, -COOMe).3.24 (s, 4H, -$CH_2CH_2$-).MALDI-Tof: *m/z* calcd for $C_{60}H_{41}N_5O_2Zn$, 927.26; found, 927.16$[M]^+$.

**9** (21 mg, 92%) $^1$H NMR (400 MHz, $CDCl_3$) δ 9.10 – 9.05 (m, 2H, pyrr-H), 8.99 – 8.91 (m, 4H, pyrrole-H), 8.91 – 8.83 (m, 2H, pyrr-H), 8.44 (dd, $J$ = 8.1, 2.1 Hz, 2H, Ar-H), 8.32 (d, $J$ = 8.1 Hz, 2H, Ar-H), 8.22 (d, $J$ = 6.6 Hz, 4H, Ar-H), 7.86 (d, $J$ = 8.3 Hz, 2H, Ar-H), 7.78 (dt, $J$ = 13.6, 6.9 Hz, 8H, Ar-H), 7.70 – 7.56 (m, 4H, Ar-H), 7.47 (t, $J$ = 7.5 Hz, 2H, Ar-H), 7.08 (s, 2H, Ar-H), 6.70 (d, $J$ = 8.5 Hz, 2H, -CH=CH-), 4.12 (d, $J$ = 4.2 Hz, 3H, -$COOCH_3$).MALDI-Tof: *m/z* calcd for $C_{60}H_{39}N_5O_2Zn$, 925.23; found, 925.13$[M]^+$.

**Synthesis of CZ-ZnP, IDB-ZnP & ISB-ZnP**

5,15-Bis(2,4,6-trimethylphenyl)-15-triphenylamino(4-methoxycarbonylphenyl)porphyrin(Zn) (16 mg, 0.018 mmol) and KOH (41 mg, 0.72 mmol) in $H_2O$ (2 mL) were added into THF-EtOH(1:1, 20 ml), and the solution was refluxed for 6 h. The mixture was then cooled to room temperature, acidified with concentrated HCl, and extracted with $CHCl_3$. The crude product left behind was then dried completely and purified with a column to afford the compound **13** (14 mg, 85%).$^1$H NMR (400 MHz, DMSO) δ 9.05 (t, $J$ = 4.2 Hz, 2H, pyrr-H), 8.87 (dd, $J$ = 4.5, 2.3 Hz, 2H, pyrr-H), 8.85 – 8.77 (m, 4H, pyrr-H), 8.48 (d, $J$ = 8.2 Hz, 2H, Ar-H), 8.44 – 8.28 (m, 6H, Ar-H), 8.21 (t, $J$ = 7.4 Hz, 4H, Ar-H), 8.07 (d, $J$ = 8.2 Hz, 2H, Ar-H), 7.96 – 7.76 (m, 8H, Ar-H), 7.62 (t, $J$ = 7.5 Hz, 2H, Ar-H), 7.42 (t, $J$ = 7.4 Hz, 2H, Ar-H).MALDI-Tof: *m/z* calcd for $C_{57}H_{35}N_5O_2Zn$,885.20; found, 885.17$[M]^+$.

**14** (14 mg, 87%).$^1$H NMR (400 MHz, DMSO) δ 8.93 – 8.85 (m, 2H), 8.76 (s, 6H), 8.36 (d, $J$ = 7.8 Hz, 2H), 8.28 (d, $J$ = 7.9 Hz, 2H), 8.18 (d, $J$ = 4.6 Hz, 4H), 7.94 (d, $J$ = 8.4 Hz, 2H), 7.80 (s, 6H), 7.70 (d, $J$ = 7.5 Hz, 2H), 7.50-7.33 (m, 6H), 6.87 (d, $J$ = 8.4 Hz, 2H).MALDI-Tof: *m/z* calcd for $C_{59}H_{39}N_5O_2Zn$, 913.23; found, 913.19$[M]^+$.

**15** (14 mg, 84%).$^1$H NMR (400 MHz, DMSO) δ 8.85 – 8.80 (m, 2H), 8.74 (m, 6H), 8.35 (d, $J$ = 8.2 Hz, 2H), 8.28 (d, $J$ = 8.1 Hz, 2H), 8.16 (dd, $J$ = 1.98, 7.07 Hz, 4H), 7.88 – 7.73 (m, 10H), 7.72 – 7.66 (m, 4H), 7.52 (t, $J$ = 7.1 Hz, 1H), 7.15 (s, 2H), 6.57 (d, $J$ = 8.6 Hz, 2H).MALDI-Tof: *m/z* calcd for $C_{59}H_{37}N_5O_2Zn$, 911.22; found, 911.16$[M]^+$.

**SYNTHESIS OF ZnP**

To a solution of ZnP-$CO_2Me$[47] (X mmol) in $CHCl_3$ (10 mL) was added excess of $Zn(OAc)_2{\cdot}2H_2O$ (32.9 mg, 150 mmol) in MeOH (3 mL). The solution was refluxed for 1 h. The solvent was removed in vacuo. This crude residue product was added to the solution of KOH (0.08 g, 0.14 mmol) dissolved in THF-EtOH-$H_2O$ (1:1:0.1, 50 mL). The solution was refluxed for 6 h. The mixture was then cooled to room temperature, acidified with concentrated HCl, and extracted with $CH_2Cl_2$. The crude product left was then dried completely and purified with a column to afford the compound **ZnP** (27.4 mg, 85%). $^1$H NMR (400 MHz, DMSO) δ: 13.24 (s, 1H, -COOH), 10.35 (s, 1H, *meso*-H), 9.49 (d, $J$ = 4.4 Hz, 2H,pyrr-H), 8.90 (d, $J$ = 4.4 Hz, 2H,pyrr-H), 8.81 (dd, $J$ = 17.3, 4.6 Hz, 4H,pyrr-H), 8.33 (dd, $J$ = 24.8, 8.1 Hz, 4H, Ar-H), 8.26 – 8.16 (m, 4H, Ar-H), 7.84 (m, 6H, Ar-H). MALDI-TOF: *m/z* calcd for $C_{39}H_{24}N_4O_2Zn$, 644.11; found, 644.01$[M]^+$.

**Acknowledgements**

This work is supported by the National Natural Science Foundation of China (no. 21076147 & no. 21476162), the Natural Science Foundation of Tianjin (no. 10JCZDJC23700), the National International S&T Cooperation Foundation of China (no. 2012DFG41980).

## Notes

[a] School of Chemical Engineering and Technology, Tianjin University, Tianjin, 300072, P. R. China. [b] Collaborative Innovation Center of Chemical Science and Engineering, Tianjin, 300072, P. R. China. [c] Department of Chemistry, University of Massachusetts Boston, 100 Morrissey Boulevard, Boston, MA 02125, United States.

Electronic Supplementary Information (ESI) available: NMR and mass spectra, TDDFT data, DFT coordinates. See DOI: 10.1039/b000000x/

## References

1. S. Ardo and G. J. Meyer, *Chem. Soc. Rev.*, 2009, **38**, 115-164.
2. A. Hagfeldt, G. Boschloo, L. Sun, L. Kloo and H. Pettersson, *Chem. Rev.*, 2010, **110**, 6595-6663.
3. B. O'Regan and M. Gratzel, *Nature*, 1991, **353**, 737-740.
4. M. Gratzel, *Inorg. Chem.*, 2005, **44**, 6841-6851.
5. P. G. Bomben, K. C. D. Robson, B. D. Koivisto and C. P. Berlinguette, *Coord. Chem. Rev.*, 2012, **256**, 1438-1450.
6. K. Hara, Z. S. Wang, Y. Cui, A. Furube and N. Koumura, *Energy Environ. Sci.*, 2009, **2**, 1109-1114.
7. A. Kay and M. Gratzel, *J. Phys. Chem.*, 1993, **97**, 6272-6277.
8. W. M. Campbell, A. K. Burrell, D. L. Officer and K. W. Jolley, *Coord. Chem. Rev.*, 2004, **248**, 1363-1379.
9. M. K. Panda, K. Ladomenou and A. G. Coutsolelos, *Coord. Chem. Rev.*, 2012, **256**, 2601-2627.
10. L.-L. Li and E. W.-G. Diau, *Chem. Soc. Rev.*, 2013, **42**, 291-304.
11. M. Urbani, M. Graetzel, M. K. Nazeeruddin and T. Torres, *Chem. Rev.*, 2014, **114**, 12330-12396.
12. V. K. Singh, R. K. Kanaparthi and L. Giribabu, *Rsc Advances*, 2014, **4**, 6970-6984.
13. A. Yella, H.-W. Lee, H. N. Tsao, C. Yi, A. K. Chandiran, M. K. Nazeeruddin, E. W.-G. Diau, C.-Y. Yeh, S. M. Zakeeruddin and M. Grätzel, *Science*, 2011, **334**, 629-634.
14. W. M. Campbell, K. W. Jolley, P. Wagner, K. Wagner, P. J. Walsh, K. C. Gordon, L. Schmidt-Mende, M. K. Nazeeruddin, Q. Wang, M. Gratzel and D. L. Officer, *J. Phys. Chem. C*, 2007, **111**, 11760-11762.
15. T. Bessho, S. M. Zakeeruddin, C.-Y. Yeh, E. W.-G. Diau and M. Graetzel, *Angew. Chem. Int. Ed.*, 2010, **49**, 6646-6649.
16. H. Imahori, Y. Matsubara, H. Iijima, T. Umeyama, Y. Matano, S. Ito, M. Niemi, N. V. Tkachenko and H. Lemmetyinen, *J. Phys. Chem. C*, 2010, **114**, 10656-10665.
17. N. Xiang, X. Huang, X. Feng, Y. Liu, B. Zhao, L. Deng, P. Shen, J. Fei and S. Tan, *Dyes Pigm.*, 2011, **88**, 75-83.
18. S. Mathew, A. Yella, P. Gao, R. Humphry-Baker, B. F. E. Curchod, N. Ashari-Astani, I. Tavernelli, U. Rothlisberger, M. K. Nazeeruddin and M. Graetzel, *Nat. Chem.*, 2014, **6**, 242-247.
19. Z.-S. Wang, Y. Cui, K. Hara, Y. Dan-oh, C. Kasada and A. Shinpo, *Adv. Mater.*, 2007, **19**, 1138-1141.

20. K. Hara, Z. S. Wang, T. Sato, A. Furube, R. Katoh, H. Sugihara, Y. Dan-Oh, C. Kasada, A. Shinpo and S. Suga, *J. Phys. Chem. B*, 2005, **109**, 15476-15482.
21. J. Wang, M. Li, D. Qi, W. Shen, R. He and S. H. Lin, *Rsc Advances*, 2014, **4**, 53927-53938.
22. Z. Yao, M. Zhang, H. Wu, L. Yang, R. Li and P. Wang, *J. Am. Chem. Soc.*, 2015.
23. C. Li and H. Wonneberger, *Adv. Mater.*, 2012, **24**, 613-636.
24. J. J. He, G. Benko, F. Korodi, T. Polivka, R. Lomoth, B. Akermark, L. C. Sun, A. Hagfeldt and V. Sundstrom, *J. Am. Chem. Soc.*, 2002, **124**, 4922-4932.
25. M. Liang and J. Chen, *Chem. Soc. Rev.*, 2013, **42**, 3453-3488.
26. R. Z. Li, M. Zhang, C. C. Yan, Z. Y. Yao, J. Zhang and P. Wang, *ChemSusChem*, 2015, **8**, 97-104.
27. N. Koumura and K. Hara, *Heterocycles*, 2013, **87**, 275-301.
28. D. M. Guldi, *Chem. Soc. Rev.*, 2002, **31**, 22-36.
29. H. Kurreck and M. Huber, *Angewandte Chemie-International Edition in English*, 1995, **34**, 849-866.
30. M. Victoria Martinez-Diaz, G. de la Torrea and T. Torres, *Chem. Comm.*, 2010, **46**, 7090-7108.
31. H. Imahori, S. Hayashi, H. Hayashi, A. Oguro, S. Eu, T. Umeyama and Y. Matano, *J. Phys. Chem. C*, 2009, **113**, 18406-18413.
32. J. M. Ball, N. K. S. Davis, J. D. Wilkinson, J. Kirkpatrick, J. Teuscher, R. Gunning, H. L. Anderson and H. J. Snaith, *Rsc Advances*, 2012, **2**, 6846-6853.
33. S. M. Feldt, E. A. Gibson, E. Gabrielsson, L. Sun, G. Boschloo and A. Hagfeldt, *J. Am. Chem. Soc.*, 2010, **132**, 16714-16724.
34. A. Aljarilla, J. N. Clifford, L. Pelleja, A. Moncho, S. Arrechea, P. de la Cruz, F. Langa and E. Palomares, *Journal of Materials Chemistry A*, 2013, **1**, 13640-13647.
35. C. Fan, X. Wang, X. Wang and J. Luo, *Optical Materials*, 2012, **34**, 609-615.
36. I. Zegkinoglou, M.-E. Ragoussi, C. D. Pemmaraju, P. S. Johnson, D. F. Pickup, J. Enrique Ortega, D. Prendergast, G. de la Torre and F. J. Himpsel, *J. Phys. Chem. C*, 2013, **117**, 13357-13364.
37. C. Wang, J. Li, S. Cai, Z. Ning, D. Zhao, Q. Zhang and J.-H. Su, *Dyes Pigm.*, 2012, **94**, 40-48.
38. B. J. Littler, Y. Ciringh and J. S. Lindsey, *J. Org. Chem.*, 1999, **64**, 2864-2872.
39. H. N. Fonda, J. V. Gilbert, R. A. Cormier, J. R. Sprague, K. Kamioka and J. S. Connolly, *J. Phys. Chem.*, 1993, **97**, 7024-7033.
40. J. Rochford, D. Chu, A. Hagfeldt and E. Galoppini, *J. Am. Chem. Soc.*, 2007, **129**, 4655-4665.
41. J. Tomasi, B. Mennucci and R. Cammi, *Chem. Rev.*, 2005, **105**, 2999-3093.
42. A. D. Becke, *J. Chem. Phys.*, 1993, **98**, 5648-5652.
43. C. T. Lee, W. T. Yang and R. G. Parr, *Physical Review B*, 1988, **37**, 785-789.
44. Harihara.Pc and J. A. Pople, *Theoretica Chimica Acta*, 1973, **28**, 213-222.
45. M. M. Francl, W. J. Pietro, W. J. Hehre, J. S. Binkley, M. S. Gordon, D. J. Defrees and J. A. Pople, *J. Chem. Phys.*, 1982, **77**, 3654-3665.
46. G. Scalmani, M. J. Frisch, B. Mennucci, J. Tomasi, R. Cammi and V. Barone, *J. Chem. Phys.*, 2006, **124**, 94107.
47. Y. Zhou, K. T. Ngo, B. Zhang, Y. Feng and J. Rochford, *Organometallics*, 2014, **33**, 7078-7090.
48. G. Boschloo and A. Hagfeldt, *Acc. Chem. Res.*, 2009, **42**, 1819-1826.
49. J. G. Rowley, B. H. Farnum, S. Ardo and G. J. Meyer, *J. Phys. Chem. Lett.*, 2010, **1**, 3132-3140.
50. J. H. Baxendale, P. L. T. Bevan and D. A. Stott, *Transactions of the Faraday Society*, 1968, **64**, 2389-2397.
51. F. Fabregat-Santiago, G. Garcia-Belmonte, I. Mora-Sero and J. Bisquert, *Phys. Chem. Chem. Phys.*, 2011, **13**, 9083-9118.
52. Q. Wang, J. E. Moser and M. Gratzel, *J. Phys. Chem. B*, 2005, **109**, 14945-14953.
53. N. Koide, A. Islam, Y. Chiba and L. Han, *Journal of Photochemistry and Photobiology a-Chemistry*, 2006, **182**, 296-305.
54. Frisch M. J. et al., *Gaussian 09*, (2009) Gaussian Inc., Wallingford, CT.
55. N. M. O'Boyle, A. L. Tenderholt and K. M. Langner, *Journal of Computational Chemistry*, 2008, **29**, 839-845.
56. M. Yanagida, T. Yamaguchi, M. Kurashige, G. Fujihashi, K. Hara, R. Katoh, H. Sugihara and H. Arakawa, *Inorg. Chim. Acta*, 2003, **351**, 283-290.
57. S. Ito, M. K. Nazeeruddin, P. Liska, P. Comte, R. Charvet, P. Pechy, M. Jirousek, A. Kay, S. M. Zakeeruddin and M. Gratzel, *Prog. Photovoltaics*, 2006, **14**, 589-601.



 